Time course and calcium dependence of transmitter release at a single ribbon synapse

Juan D. Goutman and Elisabeth Glowatzki*

Department of Otolaryngology, Head and Neck Surgery, The Johns Hopkins University School of Medicine, 720 Rutland Avenue, Ross 824, Baltimore, MD 21205

Edited by Jeremy Nathans, The Johns Hopkins University School of Medicine, Baltimore, MD, and approved August 29, 2007 (received for review June 19, 2007)

At the first synapse in the auditory pathway, the receptor potential of mechanosensory hair cells is converted into a firing pattern in auditory nerve fibers. For the accurate coding of timing and intensity of sound signals, transmitter release at this synapse must occur with the highest precision. To measure directly the transfer characteristics of the hair cell afferent synapse, we implemented simultaneous whole-cell recordings from mammalian inner hair cells (IHCs) and auditory nerve fiber terminals that typically receive input from a single ribbon synapse. During a 1-s IHC depolarization, the synaptic response depressed >90%, representing the main source for adaptation in the auditory nerve. Synaptic depression was slightly affected by α-amino-3-hydroxy-5-methyl-4-isoxazolepropionic acid receptor desensitization; however, it was mostly caused by reduced vesicular release. When the transfer function between transmitter release and Ca^{2+} influx was tested at constant open probability for Ca^{2+} channels (potentials >0 mV), a super linear relation was found. This relation is presumed to result from the cooperative binding of three to four Ca^{2+} ions at the Ca^{2+} sensor. However, in the physiological range for receptor potentials (−50 to −30 mV), the relation between Ca^{2+} influx and afferent activity was linear, assuring minimal distortion in the coding of sound intensity. Changes in Ca^{2+} influx caused an increase in release probability, but not in the average size of multivesicular synaptic events. By varying Ca^{2+} buffering in the IHC, we further investigate how Ca^{2+} channel and Ca^{2+} sensor at this synapse might relate.

hearing | exocytosis | hair cell | synaptic transmission | auditory nerve fiber

Mechanosensory hair cells of the inner ear release neurotransmitter continuously and with high temporal precision onto dendrites of auditory nerve fibers (AFs) (1); therefore, availability of releasable synaptic vesicles is critical. Synaptic ribbons, presynaptic structures presenting a halo of tethered vesicles, also found in retinal photoreceptors and bipolar cells (2), are thought to facilitate accumulation of vesicles presynaptically (3). Postsynaptically, α-amino-3-hydroxy-5-methyl-4-isoxazolepropionic acid (AMPA) receptors mediate fast synaptic transmission (4). The response of the cochlea to sound has been investigated in great detail: prolonged sound stimulation produces an increase in the firing activity of the auditory nerve that adapts on a milliseconds time scale (5). However, direct demonstration of the synaptic processes underlying adaptation and sustained release is still missing. Heretofore, hair cell exocytosis has been measured by changes in membrane capacitance that sum activity from all of the dozens of ribbon synapses in each cell (3). Capacitance measurements therefore cannot distinguish properties of individual ribbons and are limited in temporal resolution, requiring extrapolation for the earliest components. Nor does this approach reveal what role postsynaptic desensitization might play.

In mammals, each of 5–30 AFs contacts one inner hair cell (IHC) through a single, unbranched dendrite (6). In this study, we took advantage of this unique innervation pattern to characterize directly the transfer function at a single IHC ribbon synapse. We used simultaneous recordings from an IHC and an afferent terminal to discriminate the presynaptic and postsynaptic contributions to afferent fiber adaptation. These postsynaptic recordings showed that release probability, but not quantum content, is altered as a function of hair cell depolarization. We also measured directly the time and Ca^{2+} dependence of release, features that determine how signals are coded at this first, uniquely crucial synapse in the mammalian auditory pathway.

Results

Time Course of Transmitter Release. In organs of Corti excised from neonatal rat inner ear, we performed simultaneous whole-cell recordings ($n = 26$) from IHCs and AF terminals at their point of contact with the IHC (Fig. 1*A*). To investigate the time course of transmitter release, we evoked Ca^{2+} currents in IHCs by applying voltage steps to the IHC (from −89 to −29 mV for 1 s every 30 s) (Fig. 1*B1*). The afferent fiber response showed an initial peak a few milliseconds after the onset of stimulation (Fig. 1*B2*). After the initial peak, mostly single excitatory postsynaptic currents (EPSCs) occurred asynchronously throughout the whole 1-s stimulation (Fig. 1*B2 Inset*). In six AF terminals, the average size of the initial peak was 301 ± 107 pA (69 IHC depolarizations, holding potential of −84 mV), and the later asynchronous EPSCs showed a wide range of amplitudes (21–710 pA). The single EPSCs were similar to those described (4): a significant proportion exhibited fast and monophasic rise and decay times and widely varying amplitudes (Fig. 1*B2 Inset*) because of coordinate multivesicular release. Other events appeared multiphasic, and we assume that these result from less coordinate release of synaptic vesicles.

For all recordings the afferent response showed synaptic depression (Fig. 1 *B2* and *B3*). After the initial peak, the response decayed with a time course best fit with two exponentials: τ_1 of 8.8 ± 1.2 ms and τ_2 of 163 ± 37 ms, reaching a steady state of release at 6.2 ± 1.7% of the initial peak. IHC Ca^{2+} currents inactivated <20% over the same time. The reduction in Ca^{2+} current could not explain the reduction in the AF response: even if the rate of release would depend on presynaptic calcium with a power of four or five, a 20% reduction in Ca^{2+} current would only cause a 60–67% reduction of the AF response.

To determine the role of desensitization in synaptic depres-

Author contributions: J.D.G. and E.G. designed research; J.D.G. performed research; J.D.G. analyzed data; and J.D.G. and E.G. wrote the paper.

The authors declare no conflict of interest.

This article is a PNAS Direct Submission.

Abbreviations: IHC, inner hair cell; AMPA, α-amino-3-hydroxy-5-methyl-4-isoxazolepropionic acid; AF, auditory nerve fiber; EPSC, excitatory postsynaptic current; CTZ, cyclothiazide; BAPTA, 1,2-bis(2-aminophenoxy)ethane-*N*,*N*,*N*′,*N*′-tetraacetate.

*To whom correspondence should be addressed. E-mail: eglowat2@jhmi.edu.

This article contains supporting information online at www.pnas.org/cgi/content/full/0705756104/DC1.

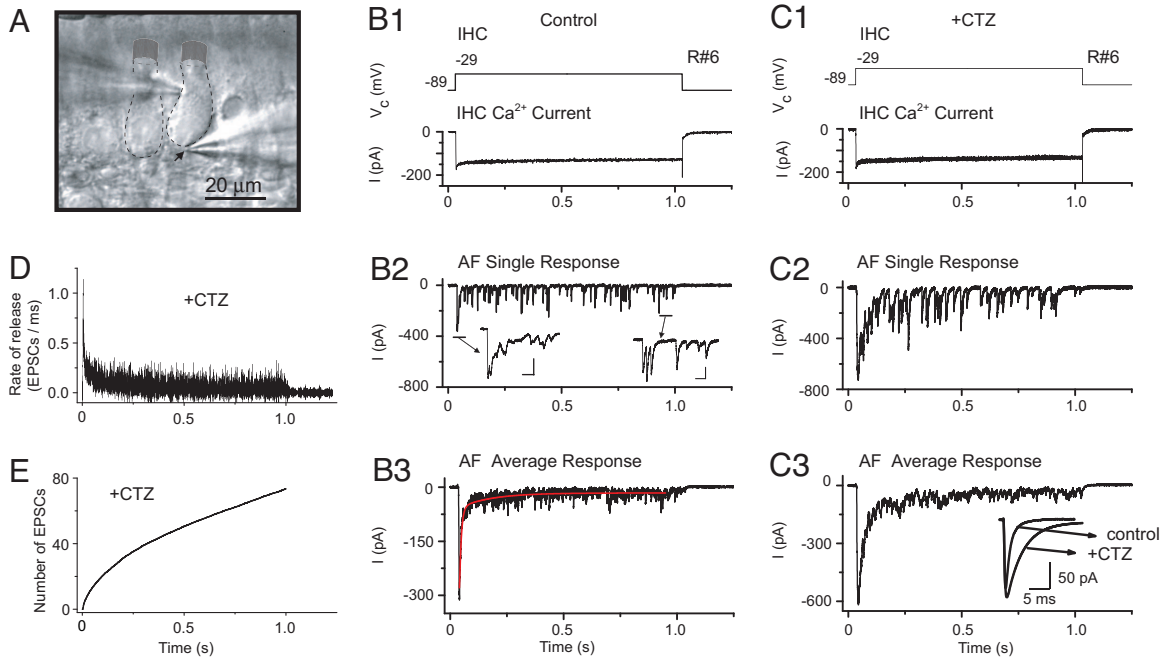

Fig. 1. Depression of AF activity during IHC depolarization mostly depends on a presynaptic mechanism. (*A*) Differential interference contrast image of the excised organ of Corti preparation; with patch pipette on the left approaching an (outlined) IHC, pipette on the right, an afferent bouton (indicated by arrow). (*B* and *C*) Simultaneous recording R6 of IHC and AF with and without 100 μM CTZ. IHC Ca^{2+} buffer contained 1 mM EGTA. (*B1* and *C1*) IHC voltage command (V_C) was applied every 30 s for 1 s and isolated IHC Ca^{2+} current. (*B2* and *C2*) AF single responses, holding potential −84 mV. (*B2 Inset*) Peak AF response and single EPSCs later in the AF response. (Scale bars: 2 ms, 50 pA.) (*B3* and *C3*) AF average responses to 13 (Control) and 12 (CTZ) depolarizations. Peak amplitudes: control, 314 ± 27 pA; CTZ, 618 ± 25 pA. Red trace, double exponential fit, τ_1 = 7.4 ms, τ_2 = 135 ms. (*C3 Inset*) Average EPSCs for R6. Control: amplitude 139 ± 7 pA, τ_{decay} 1.1 ± 0.1 ms, n = 69. CTZ: amplitude 152 ± 10 pA, τ_{decay} 3.9 ± 0.1 ms, n = 36. (*D*) Deconvolution (average of six recordings, 96 IHC depolarizations) of average AF responses with average EPSCs. (*E*) Integral of deconvolution in *D*.

sion, we compared AF responses with and without 100 μM cyclothiazide (CTZ), which removes AMPA receptor desensitization (4, 7) (n = 9, 145 IHC depolarizations) (Fig. 1*C*). In CTZ, EPSC decay times slowed down 4-fold (τ_{decay} control, 1.7 ± 0.1 ms; τ_{decay} CTZ, 7.5 ± 0.8 ms, P = 0.0005) (Fig. 1*C3 Inset*), whereas the amplitude of single EPSCs (measured during the second half of the response) did not significantly increase (control, 199 ± 45 pA, 309 EPSCs, six recordings; CTZ, 232 ± 30 pA, 265 EPSCs, nine recordings; P = 0.52). Also, the initial peak of the AF response, which results from summation of numerous EPSCs, increased by 75 ± 24% compared with control (n = 5 recordings in both experimental conditions, P = 0.035) and broadened significantly (τ_1, 27 ± 5 ms; τ_2, 264 ± 55 ms; n = 8, 145 IHC depolarizations; P = 0.008 for τ_1, P = 0.193 for τ_2). These effects on the AF response can be attributed to the loss of desensitization. We did not find any presynaptic effect of CTZ (8). CTZ affected neither Ca^{2+} currents nor the steady-state rate of release from the IHC (data not shown). We therefore conclude that AMPA receptor desensitization abbreviates the AF response. However, even after removing desensitization in CTZ, the AF response still depressed. Steady-state release was 11.0 ± 2.4% (n = 9) of the initial peak, not significantly different from control, thus confirming that synaptic depression is likely caused by presynaptic mechanisms such as vesicle depletion, as inferred previously from capacitance recordings (9–14).

To quantify further the time course of vesicle release, we deconvolved the average AF response with the waveform of the average single EPSC for each AF (in CTZ). This procedure yielded an initial rate of release of 1.1 ± 0.4 EPSCs/ms (n = 6, 96 IHC depolarizations) that exhausted within <3 ms. Fig. 1*D* shows the time course of the rate of release (EPSCs per ms), and Fig. 1*E* shows the integral of the deconvolved response, both as combined results from six AF terminals. To assign values to release dynamics, the integral was best fit by the sum of three exponentials and a linear component (see *Methods*): τ_1 = 2.1 ms, τ_2 = 18 ms, and τ_3 = 176 ms; A_1 = 1.7, A_2 = 4.2, and A_3 = 25. A_1 to A_3 provide the number of EPSCs in each component. The slope of the linear component represents sustained release (43 EPSCs per s). The entire 1-s stimulation activated 74 EPSCs.

Ca^{2+} Dependence of Release. To investigate the dependence of release on Ca^{2+} influx, the IHC membrane potential was clamped to voltages between −89 and +31 mV in 10-mV increments for 200 ms every 15 s, while the AF was held at a voltage of −84 mV (in CTZ, n = 6, two to five IHC depolarizations per voltage). IHC Ca^{2+} currents activated around −49 mV and rose to a maximum of −172 ± 18 pA around −19 mV (Fig. 2 *A1* and *B1*). The average AF response (peak or integral provide equivalent results) also activated around −49 mV and rose to a maximum value around −29 mV (Fig. 2 *A2* and *B2*). The EPSC rate (evaluated by counting EPSCs in the last 100 ms of depolarization) (Fig. 2*B3*) showed a similar voltage dependence as the peak AF response. In contrast, the average EPSC amplitude during the last 100 ms was independent of voltage and Ca^{2+} influx (Fig. 2*B3 Inset*) (seven to nine voltage steps analyzed, 4 to 48 EPSCs per potential, one-way ANOVA and Bonferroni post hoc test, $P > 0.05$ for three of four recordings; for one of four recordings significant differences were found for only two of nine voltage steps). These results show that different levels of Ca^{2+} influx change the probability of release rather than the average amplitude of multivesicular EPSCs.

We further investigated the physiologically relevant voltage range, −49 to −29 mV, in increments of 2 mV (n = 3, three to four repetitions per voltage) (Fig. 3*A*) and found a near-linear relation between Ca^{2+} influx and release with a power of 1.1 for the peak (Fig. 3*C*) and 1.4 for the integral of the AF response

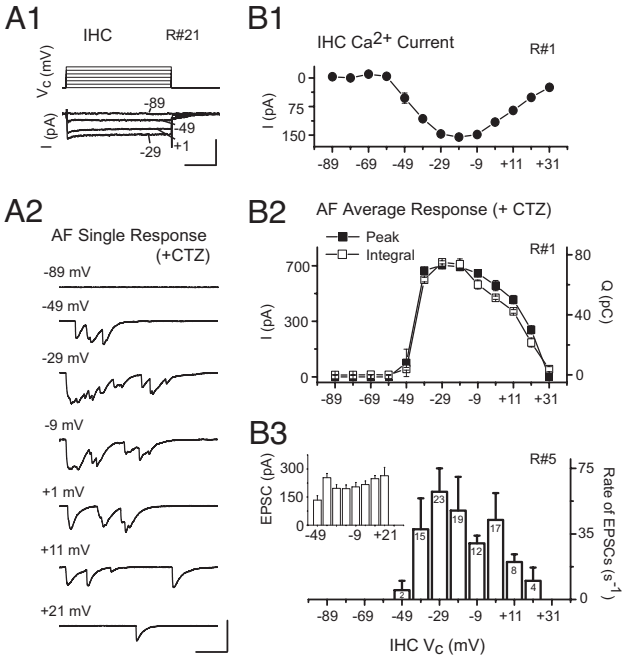

Fig. 2. Voltage and Ca^{2+} dependence of the AF response. EPSC rate, but not EPSC amplitude, is Ca^{2+}-dependent. (*A1*) IHC voltage steps protocol: −89 to +31 mV, 10-mV steps, for 200 ms and IHC Ca^{2+} currents. (Scale bar: 50 ms, 100 pA.) (*A2*) AF single responses at selected holding potentials. (Scale bars: 50 ms, 200 pA.) (*B1* and *B2*) Voltage dependence of simultaneous recordings for IHC Ca^{2+} currents (*B1*) and average AF responses (*B2*) (four repetitions per voltage, peak, or integral). (*B3*) Voltage dependence of EPSC rate and EPSC amplitude (*Inset*) for the last 100 ms of stimulation. Number of EPSCs per V_c is indicated.

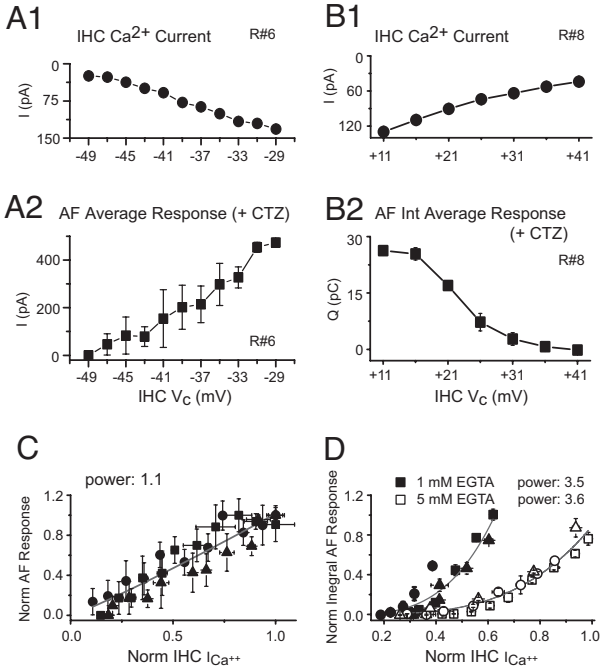

Fig. 3. The Ca^{2+} dependence of release is linear for negative IHC membrane potentials and super linear for positive IHC membrane potentials. Transfer functions between IHC Ca^{2+} current and postsynaptic response for a negative (*A1*, *A2*, and *C*) and a positive (*B1*, *B2*, and *D*) voltage range. (*A1* and *B1*) IHC Ca^{2+} current. (*A2*) AF peak response. (*B2*) AF integral response. (*C* and *D*) Ca^{2+} dependence of release for both voltage ranges; the normalized AF response was plotted versus the normalized Ca^{2+} current. Red line: fit with power function. (*C*) Symbols represent data from three cell pairs (R6, R18, and R19); five to seven voltage steps per recording, two to four repetitions per step. (*D*) Normalized integral of AF response vs. normalized Ca^{2+} current for the positive voltage range was tested in two different buffer conditions: 1 mM EGTA (filled symbols, $n = 3$ cell pairs, R4, R8, R20; five to seven voltage steps, two to four repetitions) and 5 mM EGTA (open symbols, $n = 3$ cell pairs, R10, R12, R9; five to nine steps, three to four repetitions).

(data not shown). A similar linear relation has been shown before at the hair cell synapse (11, 14–16) and explained by a "nanodomain model," where opening of one Ca^{2+} channel activates release of only very nearby vesicles (15, 17). Thus, as open probability rises with depolarization, each Ca^{2+} channel's "cluster" of vesicles sums to produce a linear dependence on Ca^{2+} current.

However, our results could also be explained if binding of calcium to the Ca^{2+} sensor occurred in a linear, rather than a cooperative, super linear fashion. To test for the intrinsic Ca^{2+} dependence of the Ca^{2+} sensor we investigated the AF response at voltage steps to positive potentials. In this voltage range, Ca^{2+} channel open probability is constant and maximal; however, the driving force for Ca^{2+} decreases at more positive potentials, and so does the single channel current (18). IHCs were voltage-clamped to values between 11 and 41 mV in 5-mV steps ($n = 3$, two to four repetitions per voltage) while Ca^{2+} current (Fig. 3*B1*) and AF response (Fig. 3*B2*) were measured. With a reduction in the Ca^{2+} current at more positive potentials, the AF response was diminished. Fig. 3*D* shows the transfer function between Ca^{2+} current and the integral of the AF response, resulting in a super linear relation with a power of 3.5. One pitfall of this experiment might be that at extreme positive potentials the very small Ca^{2+} currents could be contaminated by less permeant ions (like Cs^+ present in the IHC pipette solution). This would not be a concern for larger Ca^{2+} currents, and therefore we repeated the experiment with stronger Ca^{2+} buffering, 5 mM EGTA (Fig. 3*D*). In this case, because of the stronger buffering effect, higher Ca^{2+} influxes were required to obtain similar AF response amplitudes, and consequently a less positive range of potentials was used: −9 to +31 mV ($n = 3$, two to four repetitions per voltage). The Ca^{2+} dependence of release was similar in 5 mM EGTA (power of 3.6) compared with 1 mM EGTA. Therefore, the super linear Ca^{2+} dependence of release is presumed to result from the cooperative binding of three to four Ca^{2+} ions at the Ca^{2+} sensor.

Sensitivity of Release to Ca^{2+} Buffering. As seen in the previous experiment, buffer strength altered the efficacy of coupling between Ca^{2+} influx and release (Fig. 3*D*). Such manipulations are central to the nanodomain model, which is based in part on the differential Ca^{2+} binding rates of the Ca^{2+} buffers EGTA and 1,2-bis(2-aminophenoxy)ethane-*N*,*N*,*N*′,*N*′-tetraacetate (BAPTA). The prediction is that only the more rapidly binding BAPTA, but not EGTA, can interrupt calcium's action in a nanodomain, as has been shown for the squid giant synapse (19).

We perfused IHCs with different Ca^{2+} buffers, while monitoring the AF response to 1 s of IHC stimulation (Fig. 4). First, we analyzed the effects of Ca^{2+} buffering on the rate of EPSCs during the last 500 ms of stimulation. Compared with 1 mM EGTA (41 ± 6 EPSCs/s, $n = 8$, 122 IHC depolarizations), the EPSC rate was reduced by 56% in 5 mM EGTA (18 ± 4 EPSCs/s, $n = 5$, 72 IHC depolarizations) and further reduced (by 91%) in 5 mM BAPTA (3.6 ± 1.3 EPSCs/s, $n = 4$, 98 IHC depolarizations) (ANOVA, $P = 0.01$) (Fig. 4). In contrast, the average size of the IHC Ca^{2+} current (160–170 pA) was unchanged in different buffers ($P = 0.89$) and therefore could not account for the effect on EPSC rate. Also, the average EPSC amplitude (215–315 pA) did not significantly change ($P = 0.35$), confirming

NEUROSCIENCE

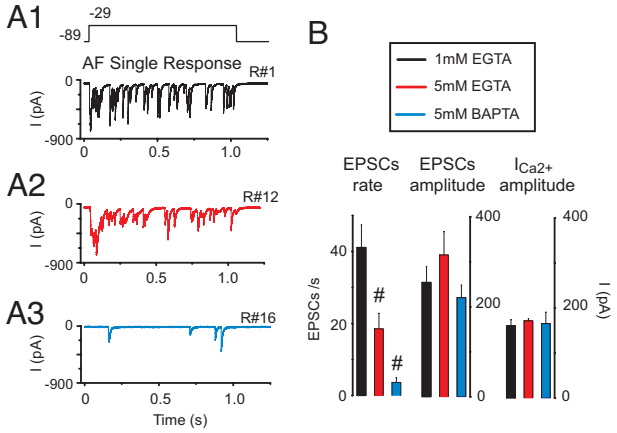

Fig. 4. The EPSC steady-state rate is sensitive to fast and slow Ca^{2+} buffering in the IHC. (*A1–A3*) Simultaneous recordings of IHCs and AFs using different IHC Ca^{2+} buffers; in 100 μM CTZ, 1-s IHC depolarization, V_c: −89 to −29 mV. (*B*) For different buffer conditions, EPSC steady-state rates were significantly different (#, $P = 0.01$), whereas EPSC amplitudes were not (1 mM EGTA: 253.9 ± 35.1 pA, $n = 6$, 179 EPSCs; 5 mM EGTA: 315 ± 51.8 pA, $n = 4$, 87 EPSCs; 5 mM BAPTA: 220 ± 27.8 pA, $n = 3$, 67 EPSCs, ANOVA, $P = 0.35$, mean values and SE). Ca^{2+} current amplitudes were not significantly different (1 mM EGTA: 160.4 ± 13.5 pA, $n = 6$, 96 depolarizations; 5 mM EGTA: 171.2 ± 4.7 pA, $n = 4$, 66 depolarizations; 5 mM BAPTA: 165.1 ± 25.3 pA, $n = 4$, 93 depolarizations, ANOVA, $P = 0.89$).

that the composition of multivesicular EPSCs does not depend on calcium (4).

Next, we analyzed the initial time course of evoked release as a function of IHC Ca^{2+} buffering. Fig. 5*A* shows the average AF responses for experiments in 1 mM EGTA ($n = 6$, 96 IHC depolarizations), 5 mM EGTA ($n = 4$, 66 IHC depolarizations), and 5 mM BAPTA ($n = 3$, 150 IHC depolarizations). In BAPTA, no initial peak was observed; instead, low-frequency EPSCs occurred throughout the 1-s IHC depolarization (Fig. 5*A1 Inset*). In 1 and 5 mM EGTA, the peak AF response was not significantly different (636 ± 88 pA and 492 ± 87 pA, $P = 0.46$). However, in 5 mM EGTA compared with 1 mM EGTA the onset of the AF response was delayed by ≈2 ms (6.1 ± 0.4 ms vs. 3.8 ± 0.2 ms, $P = 0.00024$) (Fig. 5*A2*). Also, the time from onset to peak was longer by ≈8 ms (18 ± 2.4 ms vs. 9.8 ± 2.1 ms, $P = 0.03$); this effect appeared as a loss of the initial peak of the release rate (Fig. 5*B*). The integral of the deconvolved average AF response with 5 mM EGTA was best fit with two rather than three exponentials: $\tau_1 = 27$ ms, $\tau_2 = 227$ ms, amplitudes of $A_1 = 5.6$, $A_2 = 15$ and a linear component (26 EPSCs per s) (Fig. 5*C*, red trace). Forty-seven EPSCs were activated during 1 s of stimulation. Previous studies (12, 20) using capacitance measurements showed that a slow component of release was sensitive to EGTA. Unexpectedly, using postsynaptic recordings, we find that the fastest component of release also is sensitive to buffering by EGTA.

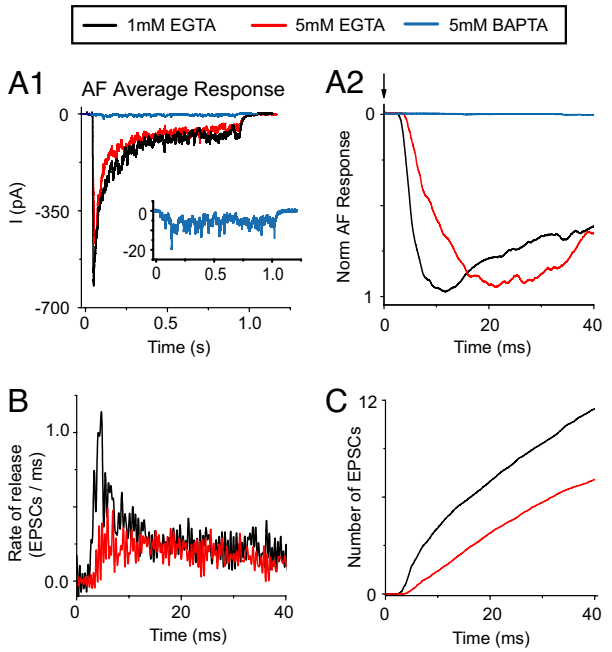

Fig. 5. Fast and slow components of release are sensitive to IHC Ca^{2+} buffering with elevated EGTA and BAPTA. (*A1*) Average AF responses in 1 mM EGTA ($n = 6$, 96 depolarizations), 5 mM EGTA ($n = 4$, 66 depolarizations), and 5 mM BAPTA ($n = 3$, 150 depolarizations, magnified in *Inset*). (*A2*) Peaks of average AF response in *A1* on extended time scale. (*B*) Deconvolution of the average AF responses in 1 and 5 mM EGTA with first 40 ms shown. (*C*) Integrals of the deconvolutions in *B*.

Discussion

Synaptic Depression. Using simultaneous recordings from IHCs and AFs, we provide a characterization of transmission at the IHC afferent synapse. During IHC depolarization the afferent response decays after an initial peak with time constants of ≈10 and 160 ms. We find that desensitization of AMPA receptors shortens single EPSCs and the peak of the afferent response. This mechanism may allow for more precise coding and signaling at higher frequencies. During the afferent response, strong synaptic depression occurs (≈90%) that persists with receptor desensitization removed. We therefore suggest that a presynaptic mechanism like reduced vesicular release must underlie synaptic depression, as inferred previously from capacitance measurements (9–14). In response to sound, the hair cell receptor potential does not adapt significantly (21); however, the firing rate of AFs adapts significantly [between 50% and 90%, as found in the mouse cochlea (22)]. Adaptation in the auditory nerve within the first second occurs in two stages: "rapid adaptation" has a time constant of a few milliseconds and "short-term adaptation" has a time constant on the order of tens of milliseconds (for review see ref. 5). Because of different experimental conditions *in vivo*, especially regarding temperature and age, these data cannot exactly be compared with our *in vitro* results. However, the features of synaptic depression found *in vitro* seem sufficient to account for the majority of auditory nerve adaptation. A future test of this hypothesis will be to record from basal AFs that adapt to a greater extent than do the presently studied apical AFs (22).

Time Course of Transmitter Release. To measure the time course of transmitter release, we used CTZ to eliminate postsynaptic effects on the afferent response. To estimate rates of release, we deconvolved the afferent response by using the waveform of the average EPSC. We found three transient components of release with time constants of ≈2, ≈18, and ≈176 ms in addition to a steady-state component. The time course of release at hair cell synapses has been thoroughly investigated by capacitance recording in different preparations, species, and ages (9–14, 20, 23). Typically, a "fast" (time constants of 2.7–53 ms) and a "slow" component of release have been found (for review see ref. 3). In general, these results are similar to those from afferent recordings. Some differences may be caused by the fact that capacitance recordings sum release from some dozen ribbon synapses per hair cell. Nevertheless, both methods find a fast component(s) of release that could represent a "readily releasable pool" of vesicles. In our hands the fastest component is released within 3 ms, and further transient release occurs within

a few 100 ms. Whether the three transient components of release provided by a fit of the afferent response are functionally distinct pools of vesicles needs to be investigated further. Second, afferent and capacitance recordings both find a component of release that does not exhaust even during 1 s of depolarization.

Numbers of Vesicles and Release Rates. To estimate the numbers of vesicles released from afferent recordings, we used the following assumptions: (*i*) We assume that the variable size of single EPSCs is caused by coordinate release of a varying number of vesicles (4, 24) and that the first peak of the EPSC amplitude distribution represents the quantal size (≈40 pA) [ref. 4 and supporting information (SI) Fig. 6] (2). A factor of seven (the average EPSC amplitude divided by the quantal size) therefore is used to convert the number of EPSCs activated into the number of vesicles released.

Based on these assumptions, we find encouraging agreement with previous estimates of ribbon function based on other methods. Thus, we calculate that the fastest component of release from a single ribbon includes 12 vesicles. Capacitance recordings from mammalian IHCs provide estimates for the fast component of 280 (12) and 680 (11) vesicles per IHC [for comparison to be divided by 10–20 ribbon synapses per IHC (25, 26)]. These numbers correlate well with electron microscopic estimates of 16 vesicles docked beneath the average ribbon in mouse IHCs (26). From our afferent recordings the transient release (all three components) includes 216 vesicles, whereas the entire 1-s stimulation activated 518 vesicles per ribbon synapse. Again, IHC capacitance recordings provide a similar estimate for the number of vesicles released per 1 s: 6,030 (12) and 7,200 (11) vesicles per IHC. Morphological data show that mouse synaptic ribbons hold ≈100–200 vesicles total (26); so that during a 1-s stimulus additional vesicles must be transported to the ribbon or directly toward the release site to support sustained release. Similarly, vesicle release monitored with a fluorescent membrane probe (27) provides an average rate of release of 1.4 vesicles per ribbon per ms for a 150-ms IHC depolarization, comparable to what we find by integrating over the same time window (1.2 vesicles per ribbon per ms).

Ca^{2+} Dependence of Release. We find a super linear Ca^{2+} dependence of release (with a power of 3.6) by using a range of positive IHC holding potentials over which single-channel currents are changed. This relation is presumed to result from the cooperative binding of three to four Ca^{2+} ions at the Ca^{2+} sensor. Similarly, using Ca^{2+} uncaging and IHC capacitance recordings, Beutner *et al.* (28) found a fifth-order Ca^{2+} dependence of release, and Brandt *et al.* (15) reported a high apparent Ca^{2+} cooperativity observed during changes of single channel currents and rapid flicker block. Our data also support the evolving picture that for the physiological relevant voltage range, hair cell synapses operate with a linear Ca^{2+} dependence of release. Similar results have been reported for the frog papilla by using simultaneous recordings from hair cells and AFs (16) and in mouse cochlea (11, 15) and turtle papilla (14) by using capacitance recordings. In the rod photoreceptor ribbon synapse a linear Ca^{2+} dependence was reported as well (29). The relation between Ca^{2+} influx and afferent activity may assure minimal distortion and high resolution for the coding of sound intensity.

An advantage of recording from the postsynaptic afferent is that it provides differentiation between two important parameters of release, the quantal content and the probability of release. This distinction enabled us to show that presynaptic Ca^{2+} current is strictly proportional to the probability of release rather than systematic changes in the amplitude of the multivesicular EPSCs. This finding marks a significant departure from earlier work concluding that *m*, the number of vesicles per release event, but not probability, is governed by Ca^{2+} influx as hair cells are depolarized (3, 30). This refinement presumably is caused by the higher temporal and spatial resolution of postsynaptic recording from single ribbon synapses that revealed the process of multivesicular release. It avoids the averaging that necessarily results when recording from multiple release sites either postsynaptically (30) or by IHC capacitance. It remains surprising that EPSC amplitude is independent of the level of Ca^{2+} influx, as also seen in earlier work (4). This Ca^{2+} independence has been further confirmed in the present work by showing that different Ca^{2+} buffers in the IHC, including 5 mM BAPTA, did not affect EPSC amplitude. How multivesicular release occurs is still unresolved and needs to be further investigated. One possibility is that compound fusion is the underlying mechanism (9, 31), as Ca^{2+}-independent forms of compound fusion have been found (32).

The linear Ca^{2+} dependence of release supports a nanodomain model for coupling between Ca^{2+} channels and synaptic vesicles. In such a model, Ca^{2+} influx through a single channel is thought to be sufficient to activate release of a nearby vesicle (Ca^{2+} sensor), located within a radius of tens of nanometers of the Ca^{2+} channel, as found in the squid giant synapse (17, 33, 34). Ca^{2+} channel open probability, P_o, undergoes a dramatic change between −49 and −29 mV. Thus, we assume that the Ca^{2+} sensor is saturated and the postsynaptic response grows in linear proportion to the presynaptic Ca^{2+} current because additional Ca^{2+} channel openings bring with them their own "unit" of vesicular release. On the contrary, in a microdomain scenario, multiple channels sum to produce a Ca^{2+} rise that reaches more distant vesicles, resulting in a super linear Ca^{2+} dependence of release as found for the calyx of Held (35, 36), where ≈60 channels open for each vesicle that is released (37, 38). In this type of synapse, release is affected by Ca^{2+} buffering with EGTA.

Surprisingly, we found an effect of EGTA on the fast component of release at the hair cell afferent synapse. In capacitance recordings the fast component of release has been shown to be insensitive to EGTA (12, 20), and in fact, 5 mM EGTA has been used to isolate the fast from the slow component (15, 26). These results are still in accordance with our data, as the amplitude of the peak AF current is not reduced in afferent recordings; however, the onset and rise time are slowed. The linear Ca^{2+} dependence of release implies that Ca^{2+} channel and Ca^{2+} sensor operate in a nanodomain. For such a model, we expected release to be insensitive to buffering with EGTA. The delay in onset and reduction in the rate of release may imply that a lower concentration of Ca^{2+} reaches the Ca^{2+} sensor in 5 mM EGTA, thereby delaying the readily releasable pool. This effect has been demonstrated at the calyx of Held, using a defined range of Ca^{2+} concentrations presynaptically (36, 37). The most straightforward interpretation of our results is that the Ca^{2+} sensor (vesicle) is located at some distance from the Ca^{2+} channel. We roughly estimated this distance at ≈23 nm, based on our result that the steady-state rate of release was reduced by ≈56% in 5 mM EGTA compared with 1 mM EGTA (SI Fig. 7). At this short distance, only one or few channel openings might still be sufficient for activating release, depending on a high-affinity Ca^{2+} sensor (28), reconciling the effect of EGTA with a nanodomain model.

Methods

IHC and AF Recordings. Excised apical turns of 9- to 11-day-old rat cochleae (Sprague–Dawley; Charles River, Wilmington, MA) were placed into a chamber under an upright microscope (Axioskop2 FS Plus; Zeiss, Oberkochen, Germany) and superfused with saline at 2–3 ml/min. IHCs and contacting AF terminals were visualized on a monitor via a ×40 water immersion objective, ×4 magnification, differential interference contrast optics with a green filter, and a Newvicon camera (Dage, MTI, Michigan City, IN).

Pipette solution for isolating IHC Ca^{2+} currents contained 135 mM $CsMeSO_3$, 13 mM tetraethyl ammonium (TEA)·Cl, 5 mM Hepes, 3.5 mM $MgCl_2$, 2.5 mM Na_2ATP, 1 or 5 mM EGTA or BAPTA, pH 7.2 (CsOH). Liquid junction potential (LJP) was 9 mV. In control experiments, 0.3 mM $CaCl_2$ was added with 5 mM EGTA ($n = 3$) or 0.05 mM $CaCl_2$ with 1 mM EGTA ($n = 1$) to the IHC pipette solution, setting a free Ca^{2+} concentration at 10–100 nM in the cytoplasm. Results were similar to experiments where no free Ca^{2+} was added. AF pipette solution contained 135 mM KCl, 3.5 mM $MgCl_2$, 0.1 mM $CaCl_2$, 5 mM EGTA, 5 mM Hepes, 2.5 mM Na_2ATP, pH 7.2 (KOH). LJP was 4 mV. Extracellular solution contained 5.8 mM KCl, 114 mM NaCl, 0.9 mM $MgCl_2$, 1.3 mM $CaCl_2$, 0.7 mM NaH_2PO_4, 5.6 mM D-glucose, 10 mM Hepes, 30 mM TEA·Cl, pH 7.4 (NaOH). Tetrodotoxin (1–5 μM) (Alomone Labs, Jerusalem, Israel) and 100 μM CTZ (Tocris, Ellisville, MO) were added depending on the experiment. All other chemicals were purchased from Sigma (St. Louis, MO).

Recording pipettes were fabricated from 1-mm borosilicate glass (WPI, Sarasota, FL), Sylgard-coated and fire-polished with tip resistances of 9–12 (AF) and 6–8 (IHC) MΩ. Series resistance errors (<4 mV for IHC Ca^{2+} currents) were not compensated for. Holding potentials were corrected for liquid junction potentials. Experiments were done at 22–24°C. Recordings were performed with a 200A and a 200B Axopatch amplifier and Digidata 1322A board (Axon Instruments, Foster City, CA), digitized at 50 kHz, and filtered at 10 kHz. Data acquisition started 5–10 min after the IHC recording (after Ca^{2+} current run-up stabilized) and lasted typically up to 40 min.

Data Analysis. Data were analyzed off-line by using pClamp, version 9.2 (Axon Instruments), Minianalysis (Synaptosoft, Decatur, GA), and Origin 7.5 (OriginLab, Northampton, MA). For leak subtraction, IHC membrane resistance was calculated from voltage steps between −89 and −69 mV. Ca^{2+} current amplitudes were measured 10 ms after the onset of IHC stimulation to minimize contamination with Na^+ currents. Na^+ currents were only partially blocked in 1 μM tetrodotoxin (TTX), but completely blocked in 5 μM TTX. If not specified in *Results*, for statistical comparison two-tailed Student's *t* test or one-way ANOVA (OriginLab) were used. Mean values are presented ± SE.

Determining the Average EPSC. EPSCs not compromised in their waveform by overlap with other events were selected by eye with a Minianalysis routine with a detection threshold of five times the rms noise. This selection was biased toward bigger EPSCs, and therefore our estimate of seven vesicles per average EPSC ($n = 6$, in CTZ: 254 ± 35 pA; $n = 179$ events) may be an overestimation compared with four to five vesicles per average EPSC found earlier, where all event had been included (ref. 4 and this work).

Deconvolution. As a prerequisite for deconvolution, we assume that the IHC afferent synapse is nonsaturating and has low occupancy of receptors. This assumption is based on the fact that we find no occlusion: for closely timed EPSCs (<5 ms peak-to-peak interval) the amplitude of the second EPSC was not systematically smaller than the amplitude of the first EPSC (E.G., unpublished work). To minimize postsynaptic effects, we used CTZ to remove desensitization of AMPA receptors. Although EPSC amplitudes at the IHC afferent synapse are highly variable, the time course of the EPSC waveform does not vary much (4), and therefore the use of the average EPSC as a template for deconvolution was appropriate. To perform deconvolution, for every simultaneous recording the Fourier transform of the AF response was divided by the Fourier transform of the average EPSC, both filtered at 2 kHz. For the result a reverse Fourier transform was performed (OriginLab). We ensured the validity of using the average EPSC for deconvolution by comparing the rate of release calculated by deconvolution with the rate of release acquired by counting EPSCs during the second half of the IHC depolarization.

Fitting the Deconvolved and Integrated AF Response. We used Eq. **1** for a fit with three exponentials and a linear component (Fig. 1*D*):

$$y = t \times c + \sum_{i}^{n} A_i(1 - \exp(-t/\tau_i)),$$

where n is the number of exponential components, A_i and τ_i are the amplitude and time constant of each component, c is a linear component, and t is the time. Fitting the 1-s-long trace, equations with two and three exponentials showed similar χ^2 values. However, the first component of release is underestimated in these fits as it is represented by a small fraction of data points comprising the 1-s trace. When we fit the first 50 ms of the trace (and removed the third exponential, only meaningful for fitting a 1-s trace), the difference between χ^2 values became obvious: χ^2/df for two exponentials and a linear component, 0.003; χ^2/df for one exponential and a linear component, 0.05 (OriginLab). Therefore, fitting with three exponentials was considered optimal.

We thank W. M. Roberts, M. A. Rutherford, and R. Schneggenburger for critical comments on the manuscript, P. A. Fuchs for discussion throughout the project and editorial comments, and S. Bandyopadhyay for advice on deconvolution analysis. This work was supported by National Institute on Deafness and Other Communication Disorders Grant DC006476 and the Human Frontiers Science Program (to E.G.).

1. Trussell LO (1999) *Annu Rev Physiol* 61:477–496.
2. Heidelberger R, Thoreson WB, Witkovsky P (2005) *Prog Retin Eye Res* 24:682–720.
3. Nouvian R, Beutner D, Parsons TD, Moser T (2006) *J Membr Biol* 209:153–165.
4. Glowatzki E, Fuchs PA (2002) *Nat Neurosci* 5:147–154.
5. Ruggero M (1992) in *The Mammalian Auditory Pathway: Neurophysiology*, eds Fay R, Popper AN (Springer, New York), pp 34–93.
6. Slepecky N (1996) in *The Cochlea*, eds Dallos P, Popper A, Fay R (Springer, New York), pp 44–129.
7. Partin KM, Patneau DK, Winters CA, Mayer ML, Buonanno A (1993) *Neuron* 11:1069–1082.
8. Ishikawa T, Takahashi T (2001) *J Physiol (London)* 533:423–431.
9. Edmonds BW, Gregory FD, Schweizer FE (2004) *J Physiol (London)* 560:439–450.
10. Eisen MD, Spassova M, Parsons TD (2004) *J Neurophysiol* 91:2422–2428.
11. Johnson SL, Marcotti W, Kros CJ (2005) *J Physiol (London)* 563:177–191.
12. Moser T, Beutner D (2000) *Proc Natl Acad Sci USA* 97:883–888.
13. Rutherford MA, Roberts WM (2006) *Proc Natl Acad Sci USA* 103:2898–2903.
14. Schnee ME, Lawton DM, Furness DN, Benke TA, Ricci AJ (2005) *Neuron* 47:243–254.
15. Brandt A, Khimich D, Moser T (2005) *J Neurosci* 25:11577–11585.
16. Keen EC, Hudspeth AJ (2006) *Proc Natl Acad Sci USA* 103:5537–5542.
17. Neher E (1998) *Neuron* 20:389–399.
18. Rodriguez-Contreras A, Yamoah EN (2001) *J Physiol (London)* 534:669–689.
19. Adler EM, Augustine GJ, Duffy SN, Charlton MP (1991) *J Neurosci* 11:1496–1507.
20. Spassova MA, Avissar M, Furman AC, Crumling MA, Saunders JC, Parsons TD (2004) *J Assoc Res Otolaryngol* 5:376–390.
21. Palmer AR, Russell IJ (1986) *Hear Res* 24:1–15.
22. Taberner AM, Liberman MC (2005) *J Neurophysiol* 93:557–569.
23. Parsons TD, Lenzi D, Almers W, Roberts WM (1994) *Neuron* 13:875–883.
24. Singer JH, Lassova L, Vardi N, Diamond JS (2004) *Nat Neurosci* 7:826–833.
25. Francis HW, Rivas A, Lehar M, Ryugo DK (2004) *Brain Res* 1016:182–194.
26. Khimich D, Nouvian R, Pujol R, Tom Dieck S, Egner A, Gundelfinger ED, Moser T (2005) *Nature* 434:889–894.
27. Griesinger CB, Richards CD, Ashmore JF (2005) *Nature* 435:212–215.
28. Beutner D, Voets T, Neher E, Moser T (2001) *Neuron* 29:681–690.
29. Thoreson WB, Rabl K, Townes-Anderson E, Heidelberger R (2004) *Neuron* 42:595–605.
30. Furakawa T, Kuno M, Matsuura S (1982) *J Physiol (London)* 332:181–195.
31. Parsons TD, Sterling P (2003) *Neuron* 37:379–382.
32. Pickett JA, Edwardson JM (2006) *Traffic* 7:109–116.
33. Augustine GJ (2001) *Curr Opin Neurobiol* 11:320–326.
34. Oheim M, Kirchhoff F, Stuhmer W (2006) *Cell Calcium* 40:423–439.
35. Bollmann JH, Sakmann B, Borst JG (2000) *Science* 289:953–957.
36. Schneggenburger R, Neher E (2000) *Nature* 406:889–893.
37. Borst JG, Sakmann B (1996) *Nature* 383:431–434.
38. Ohana O, Sakmann B (1998) *J Physiol (London)* 513:135–148.